Check for updates

A series of planar tetranuclear lanthanide complexes: axial ligand modulated magnetic dynamics in Dy$_4$ species†

Ya-Xin Zhang,[a] Meng Li,[a] Bi-Ying Liu,[a] Zhi-Lei Wu, [iD] *[a] Hai-Ying Wei*[a] and Wen-Min Wang*[b]

Ten new lanthanide compounds were successfully obtained based on an 8-hydroxyquinoline Schiff base derivative and β-diketonates with different substituent groups, namely, [Ln$_4$(μ$_3$-OH)$_2$L$_6$(acac)$_4$]·2.5CH$_3$CN (Ln = Gd (**1**), Tb (**2**), Dy (**3**), Ho (**4**) and Yb (**5**); HL = 5-(4-methoxybenzylidene)-8-hydroxylquinoline; Hacac = acetylacetone), [Ln$_4$(μ$_3$-OH)$_2$L$_6$(tmhd)$_4$]·xCH$_3$CN·yCH$_3$CH$_2$OH (Ln = Eu (**6**), Gd (**7**), and Tb (**8**), x = 1, y = 1; Ln = Dy (**9**), x = 2, y = 0; Htmhd = 2,2,6,6-tetramethyl-3,5-heptanedione) and [Dy$_4$(μ$_3$-OH)$_2$L$_6$(beac)$_4$]·CH$_3$CN (**10**) (Hbeac = 1-benzoylacetone). Single crystal X-ray diffraction revealed that compounds **1**–**10** all contain planar tetranuclear lanthanide centers with a similar butterfly-shape arrangement, and each lanthanide ion is located in a distorted bicapped trigonal prism coordination sphere. **1**·Gd and **7**·Gd exhibit magnetic refrigeration behavior with the maximum values of $-\Delta S_m$ being 19.39(2) and 16.21(3) J K^{-1} kg^{-1}, respectively. Additionally, the effects of steric-hindrance on the magnetic anisotropy of the Dy^{3+} centers in **3**·Dy, **9**·Dy and **10**·Dy were observed through comparative studies on their magnetic behaviors, which showed different SMM behaviors with energy barriers of 99.29(3) K for **3**·Dy, 64.56(4) K for **9**·Dy and 61.05(0) K for **10**·Dy.

Introduction

Single molecule magnets (SMMs) have become more and more attractive in the fields of chemistry, physics and materials science in that they show potential optical applications and quantum phenomena.[1–3] A number of SMMs have been reported in recent years,[4–7] especially for lanthanide-based magnetic compounds, many of which display intriguing magnetic behaviors due to the significant intrinsic magnetic anisotropy arising from their large and unquenched orbital angular momentum. However, intentional design and regulation of structural and magnetic changes is still a challenge. The investigations reveal that the magnetic properties can be deliberately tuned by altering the coordination geometry and ligand field around the metal centers. It should be noted that the regulation of magnetic transformations has been realized by changing the solvent molecules,[8] doping with other elements,[9] modifying ligands,[10] *etc.* Impressively, Tong's group synthesized two similar dysprosium complexes coordinated by different

peripheral anions (Cl$^-$ and Br$^-$), displaying distinct magnetic dynamics with effective energy barriers of 708 K and 1025 K, respectively.[11] In addition, two dinuclear dysprosium compounds with different magnetic properties were assembled by Tang *et al.* through employing two ligands with different coordination pockets.[12] Hence, it can be seen that the SMMs behaviors were sensitive to the coordination geometry and ligand fields around the lanthanide sites, and even a slight change in the coordination environment of Ln(III) ion center might result in significant divergence of the magnetic behaviors.

In our previous work, we employed two Schiff base ligands with different substituents to construct SMMs, and investigated the electronic effect on the magnetic behaviors, obtaining two dysprosium complexes with anisotropic barriers ($\Delta E/k_BT$) 67.6 K and 34.5 K, respectively.[13] The different SMMs behaviors mainly originated from the different electron-donating effect, which to some extent influenced the coordination environment of center Dy^{3+} ions. Inspired by this case, we expect to prepare different series of lanthanide complexes based on Schiff base ligand HL (HL = 5-(4-methoxybenzylidene)-8-hydroxylquinoline; synthesized by condensation of 5-amino-8-hydroxyquinoline and 4-methoxybenzaldehyde) and different β-diketonates (Scheme 1 and 2) with objective to study the effect of auxiliary ligands on both structures and magnetic properties. Herein, as a continuation of our work, we report three series of tetranuclear lanthanide complexes with similar butterfly topology based on HL and β-diketonates, [Ln$_4$(μ$_3$-OH)$_2$L$_6$(acac)$_4$]·2.5CH$_3$CN (Ln =

^{a}*College of Chemistry and Environmental Science, Hebei University, Baoding, 071002, P. R. China. E-mail: wuzhilei03@163.com; weihy@hbu.edu.cn*

^{b}*Department of Chemistry, Tianjin University, Tianjin, 300072, China. E-mail: wangwenmin0506@126.com*

Gd (**1**), Tb (**2**), Dy (**3**), Ho (**4**) and Yb (**5**); Hacac = acetylacetone), [Ln$_4$(μ_3-OH)$_2$L$_6$(tmhd)$_4$]·xCH$_3$CN·yCH$_3$CH$_2$OH (Ln = Eu (**6**), Gd (**7**), and Tb (**8**), $x = 1$, $y = 1$; Ln = Dy (**9**), $x = 2$, $y = 0$; Htmhd = 2,2,6,6-tetramethyl-3,5-heptanedione) and [Dy$_4$(μ_3-OH)$_2$L$_6$-(beac)$_4$]·CH$_3$CN (**10**) (Hbeac = 1-benzoylacetone). Thereinto, complexes **3**·Dy, **9**·Dy and **10**·Dy display different magnetic relaxation behaviors with the energy barrier of 99.29(3) K for **3**·Dy, 64.56(4) K for **9**·Dy and 61.05(0) K for **10**·Dy. As expected, their magnetic properties show a substituent-dependent phenomenon, which mainly originate from the different ligand field effects on the local Dy^{3+} sites. Additionally, complexes **1**·Gd and **7**·Gd exhibit magnetic entropy change ($-\Delta S_m$) of 19.39(2) J K^{-1} kg^{-1} and 16.21(3) J K^{-1} kg^{-1}, respectively.
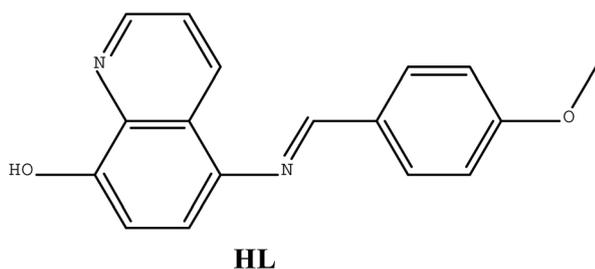
Experiment section

Materials and general methods

All the chemicals and solvents used for the syntheses were reagent grade without further purification. The Ln(acac)$_3$·2H$_2$O (Ln = Gd, Tb, Dy, Ho, Yb), Ln(tmhd)$_3$·2H$_2$O (Ln = Eu, Gd, Tb, Dy) and Dy(heac)$_3$·2H$_2$O were obtained according to the literature previously.[14] The Schiff base ligand HL was synthesized by condensation of 5-amino-8-hydroxyquinoline and 4-methoxybenzaldehyde. ^{1}H NMR spectra was performed on JEOL Eclipse β 400 MHz spectrometer. Elemental analyses for C, H and N were measured by a PerkinElmer 240 CHN elemental analyzer. IR spectra were recorded on a Bruker Tensor 27 spectrophotometer using KBr disks. Powder X-ray diffraction (PXRD) data were collected on a D/Max-2500 X-ray diffractometer using Cu Kα radiation (Fig. S3 in ESI†). Thermogravimetric analysis (TGA) was performed on a Netzsch TG 209 Setaram apparatus from room temperature to 800 °C with a heating rate of 10 °C min^{-1} (Fig. S4 in ESI†). Magnetic measurements were carried out with Quantum Design MPMS-XL7 and PPMS-9 ACMS magnetometers. All the samples were restrained in eicosane to prevent torqueing. The diamagnetic corrections for compounds were estimated from Pascal's constants as well as sample holder calibration.

Crystallographic studies

Single-crystal X-ray diffraction measurements of **1–10** were collected on a Rigaku-RAPID diffractometer equipped with graphite-monochromatic Mo Kα radiation (λ = 0.71073 Å). The structures were solved by direct methods and refined by full-

matrix least-squares methods on F^2 using SHELXTL-97 and SHELXTL-97 programs. All non-hydrogen atoms were refined with anisotropic parameters, while hydrogen atoms were placed in calculated positions and refined using a riding model. Due to the low residual electron density, the position of free solvents cannot be determined by single crystal X-ray diffraction techniques, and therefore the SQUEEZE routine in the PLATON software package was applied. Crystallographic data parameters for **1–10** are listed in Tables S1 and S2.† CCDC 1544673–1544682† contain supplementary crystallographic data for compounds **1–10**.

Results and discussion

Synthesis and IR spectra

Preparation of HL. A solution of 5-amino-8-hydroxyquinoline (0.5 mmol) and 4-methoxybenzaldehyde (0.5 mmol) in the 30 mL methanol was stirred for 4 h at room temperature. Then the reaction product was filtered and dried at 50 °C for 5 h. It can be confirmed by IR spectrum (Fig. 1). For example, the broad peak at 3349 cm^{-1} can be ascribed to the O–H stretching vibration of 8-hydroxyquinoline, weak 3072 cm^{-1} peak and the strong 1603 cm^{-1} peak are the stretching vibration of =C–H and C=N group, the 2836 cm^{-1} peak can be assigned to the C–H stretching vibration of O–CH$_3$ group. Furthermore, the peak at 1236 cm^{-1} represents the C–O stretching vibration of phenol hydroxyl group.

Preparation of compounds 1–5. A mixture of Ln(acac)$_3$·2H$_2$O (0.02 mmol; Ln = Gd, Tb, Dy, Ho, Yb) and HL (0.02 mmol) were dissolved in 15 mL acetonitrile and 5 mL CH$_2$Cl$_2$. Then the obtaining yellow solution was stirred for 3 h at room temperature. After filtration, the resultant solution was kept unperturbed to evaporate slowly. After 7 days, yellow needle-shaped crystals suitable for single-crystal X-ray diffraction analysis were obtained.

[Gd$_4$(μ_3-OH)$_2$L$_6$(acac)$_4$]·2.5CH$_3$CN (**1**·Gd). Yield based on Gd: 38%. IR (KBr, cm^{-1}): 3693 (s), 3631 (w), 2916 (w), 2836 (w), 1602 (s), 1573 (w), 1515 (m), 1499 (m), 1464 (m), 1384 (m), 1357 (w), 1310 (m), 1253 (w), 1165 (m), 1090 (m), 1019 (w), 833 (m), 919 (w), 881 (w), 832 (w), 787 (w), 760 (w), 525 (w). Anal. calcd for C$_{127}$H$_{115.5}$N$_{14.5}$O$_{22}$Gd$_4$: C, 53.98; H, 4.10; N, 6.94. Found: C, 54.13; H, 4.25; N, 6.78.

[Tb$_4$(μ_3-OH)$_2$L$_6$(acac)$_4$]·2.5CH$_3$CN (**2**·Tb). Yield based on Tb: 42%. IR (KBr, cm^{-1}): 3693 (s), 3631 (w), 2915 (w), 2836 (w), 1601 (s), 1573 (w), 1515 (m), 1498 (m), 1464 (m), 1384 (m), 1356 (w), 1310 (m), 1252 (w), 1165 (m), 1090 (m), 1019 (w), 833 (m), 918 (w), 881 (w), 831 (w), 787 (w), 760 (w), 524 (w). Anal. calcd for C$_{127}$H$_{115.5}$N$_{14.5}$O$_{22}$Tb$_4$: C, 53.85; H, 4.09; N, 6.92. Found: C, 53.63; H, 3.92; N, 7.07.

[Dy$_4$(μ_3-OH)$_2$L$_6$(acac)$_4$]·2.5CH$_3$CN (**3**·Dy). Yield based on Dy: 37%. IR (KBr, cm^{-1}): 3693 (s), 3630 (w), 2916 (w), 2836 (w), 1601 (s), 1573 (w), 1514 (m), 1499 (m), 1464 (m), 1384 (m), 1356 (w), 1310 (m), 1253 (w), 1166 (m), 1090 (m), 1019 (w), 832 (m), 919 (w), 881 (w), 832 (w), 788 (w), 760 (w), 525 (w). Anal. calcd for C$_{127}$H$_{115.5}$N$_{14.5}$O$_{22}$Dy$_4$: C, 53.58; H, 4.07; N, 6.89. Found: C, 53.71; H, 4.19; N, 6.72.

[Ho$_4$(μ_3-OH)$_2$L$_6$(acac)$_4$]·2.5CH$_3$CN (**4**·Ho). Yield based on Ho: 57%. IR (KBr, cm^{-1}): 3693 (s), 3631 (w), 2916 (w), 2835 (w), 1602
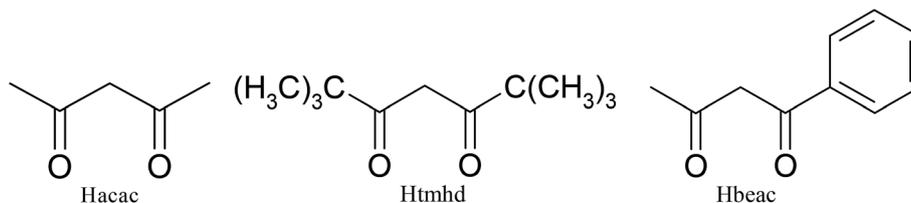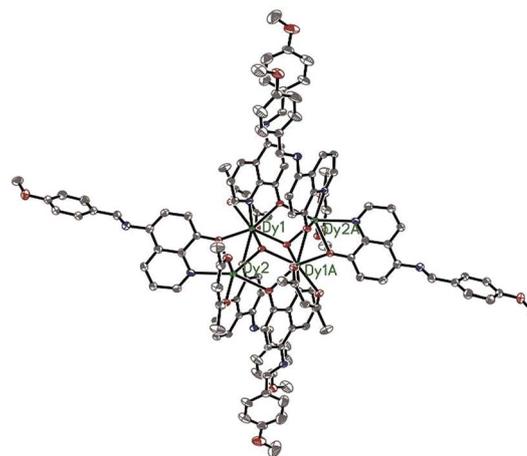

Scheme 1 Structure of ligand HL.

Scheme 2   Structures of three different β-diketones.
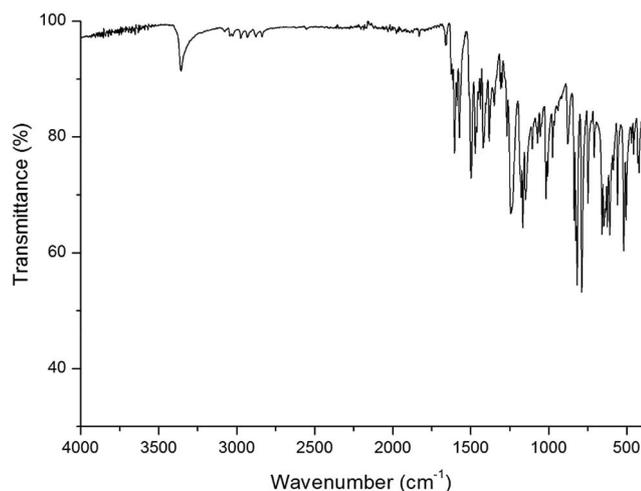
Fig. 1   The IR spectrum of ligand HL.

(s), 1573 (w), 1514 (m), 1498 (m), 1464 (m), 1384 (m), 1357 (w), 1311 (m), 1253 (w), 1165 (m), 1090 (m), 1018 (w), 833 (m), 919 (w), 881 (w), 831 (w), 787 (w), 760 (w), 525 (w). Anal. calcd for $C_{127}H_{115.5}N_{14.5}O_{22}Ho_4$: C, 53.40; H, 4.06; N, 6.86. Found: C, 53.25; H, 4.15; N, 6.72.

   [Yb₄(μ₃-OH)₂L₆(acac)₄]·2.5CH₃CN (5·Yb). Yield based on Yb: 61%. IR (KBr, cm⁻¹): 3693 (s), 3632 (w), 2916 (w), 2836 (w), 1602 (s), 1572 (w), 1515 (m), 1499 (m), 1464 (m), 1383 (m), 1357 (w), 1310 (m), 1252 (w), 1165 (m), 1091 (m), 1019 (w), 833 (m), 919 (w), 881 (w), 833 (w), 787 (w), 760 (w), 525 (w). Anal. calcd for $C_{127}H_{115.5}N_{14.5}O_{22}Yb_4$: C, 52.80; H, 4.01; N, 6.79. Found: C, 52.66; H, 3.89; N, 6.88.

   Preparation of compounds 6–9. The reaction mixture of HL (0.02 mmol) and Ln(tmhd)₃·2H₂O (0.02 mmol; Ln = Eu, Gd, Tb, Dy) in acetonitrile and ethanol (15 mL/5 mL) mixture solution was stirred at room temperature for 3 h. After filtration, the resultant solution was left unperturbed to evaporate slowly, producing yellow block shaped crystals **6–9** after 6 days.

   [Eu₄(μ₃-OH)₂L₆(tmhd)₄]·CH₃CN·CH₃CH₂OH (6·Eu). Yield based on Eu: 35%. IR (KBr, cm⁻¹): 3434 (s), 2958 (w), 2922 (w), 2838 (w), 1603 (s), 1573 (m), 1515 (m), 1464 (m), 1387 (m), 1309 (m), 1251 (m), 1165 (m), 1134 (w), 1091 (m), 1023 (m), 921 (w), 833 (m), 786 (m), 760 (m), 718 (w), 657 (w), 591 (w), 525 (w). Anal. calcd for $C_{154}H_{174}N_{14}O_{24}Eu_4$: C, 57.57; H, 5.46; N, 6.10. Found: C, 57.67; H, 5.27; N, 6.22.

   [Gd₄(μ₃-OH)₂L₆(tmhd)₄]·CH₃CN·CH₃CH₂OH (7·Gd). Yield based on Gd: 44%. IR (KBr, cm⁻¹): 3433 (s), 2958 (w), 2922 (w), 2837 (w), 1603 (s), 1572 (m), 1516 (m), 1464 (m), 1387 (m), 1310

Fig. 2   The molecular structure of compound **3**·Dy (top) and the butterfly shaped tetranuclear Dy(III) center in **3**·Dy (bottom). Hydrogen atoms are omitted for clarity (Dy green; C gray; N blue; O red).

(m), 1251 (m), 1165 (m), 1135 (w), 1091 (m), 1023 (m), 920 (w), 833 (m), 786 (m), 761 (m), 718 (w), 656 (w), 590 (w), 525 (w). Anal. calcd for $C_{154}H_{174}N_{14}O_{24}Gd_4$: C, 57.19; H, 5.42; N, 6.06. Found: C, 57.06; H, 5.53; N, 6.13.

   [Tb₄(μ₃-OH)₂L₆(tmhd)₄]·CH₃CN·CH₃CH₂OH (8·Tb). Yield based on Tb: 46%. Elemental analysis (%) calcd for IR (KBr, cm⁻¹): 3433 (s), 2958 (w), 2921 (w), 2837 (w), 1602 (s), 1572 (m), 1515 (m), 1464 (m), 1388 (m), 1310 (m), 1251 (m), 1164 (m), 1135 (w), 1091 (m), 1023 (m), 920 (w), 833 (m), 787 (m), 761 (m), 718 (w), 655 (w), 590 (w), 525 (w). Anal. calcd for $C_{154}H_{174}N_{14}O_{24}Tb_4$: C, 57.07; H, 5.41; N, 6.05. Found: C, 56.88; H, 5.56; N, 5.94.

[Dy₄(μ₃-OH)₂L₆(tmhd)₄]·2CH₃CN (9·Dy). Yield based on Dy: 51%. Elemental analysis (%) calcd for IR (KBr, cm⁻¹): 3433 (s), 2958 (w), 2921 (w), 2837 (w), 1602 (s), 1572 (m), 1516 (m), 1464 (m), 1387 (m), 1311 (m), 1251 (m), 1164 (m), 1135 (w), 1091 (m), 1023 (m), 921 (w), 833 (m), 786 (m), 762 (m), 718 (w), 656 (w), 591 (w), 525 (w). Anal. calcd for $C_{154}H_{168}N_{16}O_{22}Dy_4$: C, 57.00; H, 5.22; N, 6.91. Found: C, 56.86; H, 5.34; N, 6.79.

Preparation of compounds 10·Dy. The synthesis of **10·Dy** was carried out following a similar procedure of **1–5** as described above, in which Dy(beac)₃·2H₂O was used instead of Ln(acac)₃·2H₂O. Strip-typed crystals were obtained from the solution after 7 days.

[Dy₄(μ₃-OH)₂L₆(beac)₄]·CH₃CN (10·Dy). Yield based on Dy: 38%. Elemental analysis (%) calcd for. IR (KBr, cm⁻¹): 3633 (s), 2963 (w), 2929 (w), 2869 (w), 1605 (s), 1570 (m), 1518 (m), 1500 (m), 1465 (m), 1404 (m), 1385 (m), 1357 (m), 1313 (m), 1263 (w), 1242 (w), 1174 (w), 1092 (m), 1055 (m), 1017 (w), 967 (w), 919 (w), 880 (w), 831 (w), 784 (w), 754 (w), 655 (w), 529 (w), 403 (w). Anal. calcd for $C_{150}H_{128}N_{16}O_{22}Dy_4$: C, 57.07; H, 4.09; N, 7.10. Found: C, 56.92; H, 4.01; N, 7.26.

Crystal structure of 1–5

Single X-ray crystal structure analysis reveal that compounds **1–5** are isostructural and crystallize in the triclinic crystal system, $P\bar{1}$ space group. Thus, compound **3·Dy** as a representative example is selected to describe in detail. As shown in Fig. 2 and 5, each molecule of **3·Dy** contains a butterfly shaped [Dy₄O₂] core, in which two μ₃-OH atoms lie 0.9064(1) Å above and below

the [Dy₄] plane, bridging the body ions (Dy1 and Dy1A) to the wingtip ions (Dy2 and Dy2A), and the four Dy ions are further linked together by four phenoxide oxygen atoms (O3, O5, O3A and O5A). The [Dy₄] core is compose of two scalene triangular, and the distance of Dy1···Dy2, Dy1A···Dy2 and Dy1···Dy1A are 3.8702(2), 3.5171(0) and 3.8668(3) Å, respectively. The periphery of [Dy₄] core is surrounded by six L⁻ and four bidentate acac⁻. All the L⁻ adopt μ_2–$\eta^2\eta^1$ bonding mode (Scheme S1†), they coordinate with Dy³⁺ ions through two donor atoms (phenoxo-O atom and N atom), and the phenoxo-O atom can also act as a bridge between two Dy³⁺ ions. Hence, one HL can bridge two Dy³⁺ ions. Moreover, due to the strong π–π interactions between the quinoline part of L⁻, four L⁻ ligands are almost in parallel arrangement and locate at different side of the Dy³⁺ ions. Meanwhile, the acac⁻ adopt η^1:η^1 bonding mode, blocking the extension of the Dy³⁺ ions, sequentially resulting into the formation of isolated tetranuclear Dy³⁺ cluster. In the asymmetric unit of **3·Dy**, the eight-coordinated Dy1 ion is coordinated by seven O atoms (two O atoms from acac⁻, two μ₃-OH and three phenoxide oxygen atoms) and one N atom, while the coordination environment of Dy2 ion is completed by six O atoms (two O atoms from acac⁻, one μ₃-OH and three phenoxide oxygen atoms) and two N atoms from L⁻. Both of them display distorted bicapped trigonal prism coordination geometry (Fig. S1†). All the lengths of Dy–O bonds fall into the range of 2.285(2)–2.411(2) Å, and the range of Dy–N distance are 2.514(3)–2.568(3) Å. Additionally, the Ln—Ln distances gradually shorten with the decrease in the ionic radius of the Ln³⁺
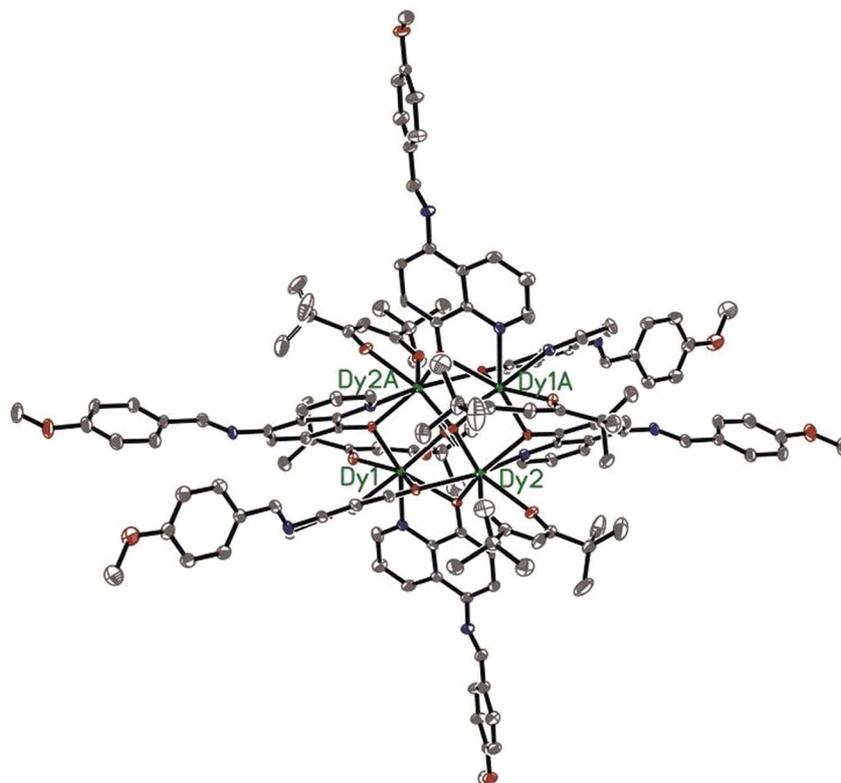

Fig. 3 The molecular structure of compound 9·Dy. Hydrogen atoms are omitted for clarity (Dy green; C gray; N blue; O red).

ions, while the Ln–O–Ln bond angles gradually increase accordingly.

Crystal structure of 6–10

Compounds **6–9** are also isostructural and isolated tetranuclear clusters, crystallizing in the $P\bar{1}$ space group, triclinic crystal system. While **10**·Dy crystallizes in the $P2_1/c$ space group, in monoclinic crystal system, it also displays a butterfly motif. So compound **9**·Dy and **10**·Dy are selected as an example to describe the structure. Comparably, the structure of **9**·Dy and **10**·Dy are similar with **3**·Dy, and they all consists of a butterfly shaped $[Dy_4O_2]$ core and six coordinated ligands L^- (Fig. 3 and 4). Differently, the coordinated bidentate β-diketonates in **9**·Dy and **10**·Dy are tmhd$^-$ and beac$^-$, respectively, instead of acac$^-$ (Fig. 5). The coordination sphere around Dy1 and Dy2 in **9**·Dy and **10**·Dy are analogous to that in **3**·Dy, exhibiting distorted bicapped trigonal prism coordination geometry (Fig. S1 in ESI†). The Dy–O bond lengths of **9**·Dy and **10**·Dy are in the range of 2.285(3)–2.415(3) Å and 2.323(6)–2.467(7) Å, and Dy–N bond distances of them are 2.533(4)–2.555(4) Å and 2.529(1)–2.546(2) Å. As for the distance between Dy ions in them, for **9**·Dy, the distance of Dy1···Dy2, Dy1A···Dy2 and Dy2···Dy2A are 3.5504(3), 3.8696(3) and 3.8963(4) Å. For **10**·Dy, the distance of Dy1···Dy2, Dy1A···Dy2 and Dy1···Dy1A are 3.8712(9), 3.6107(1) and 3.8816(1) Å. The crystal packing of compounds **3**·Dy, **9**·Dy and **10**·Dy show that the molecules contact each other through strong π–π interactions, thus generating an infinite supramolecular chains in them (Fig. S2 in ESI†). Finally, these supramolecular chain in **3**·Dy, **9**·Dy and **10**·Dy are stacked through

weak intermolecular H-bonding interactions between free solvent molecules locating in their crystal lattices.

The structural differences among **3**·Dy, **9**·Dy and **10**·Dy can be attributed to the strengths and symmetries of the three β-diketonate coligands. Meanwhile, the introduction of different substituent groups, to some extent, may changes the ligand field strength of Ln ion centers, thus further affecting their magnetic behaviors.

Magnetic properties

The solid-state temperature-dependent magnetic susceptibilities of compounds **1–10** were investigated in the range of 2–300 K under an applied magnetic field of 1000 Oe using the crystalline aggregates (Fig. 6).

At room temperature, the $\chi_M T$ values for compounds **1–5** are 31.08 (**1**·Gd), 47.74 (**2**·Tb), 56.87 (**3**·Dy), 56.02 (**4**·Ho) and 10.78 (**5**·Yb) cm^3 K mol^{-1}, which are very close to the theoretical values of 31.52, 47.28, 56.68, 56.28 and 10.28 cm^3 K mol^{-1}, calculated based on four isolated Gd^{3+} ($^8S_{7/2}$, $g = 2$), Tb^{3+} ($^7F_6$, $g = 3/2$), Dy^{3+} ($^6H_{15/2}$, $g = 4/3$), Ho^{3+} ($^5I_8$, $g = 5/4$), Yb^{3+} ($^2F_{7/2}$, $g = 8/7$), respectively. Upon cooling, the $\chi_M T$ values of **1–4** decrease slowly from 300–50 K, and then decline rapidly to minimum values of 14.40, 33.62, 31.60, 27.27 cm^3 K mol^{-1} at 2 K. In the case of **5**·Yb, the $\chi_M T$ value gradually decreases to 4.44 cm^3 K mol^{-1}. These magnetic behaviors are generally ascribed to the thermal depopulation of the Ln^{3+} excited Stark sublevels resulting from the spin–orbit coupling and/or weak antiferromagnetic interactions between Ln^{3+} ions.[15] For compounds **6**·Eu, the $\chi_M T$ values is 5.07 cm^3 K mol^{-1} at room temperature,
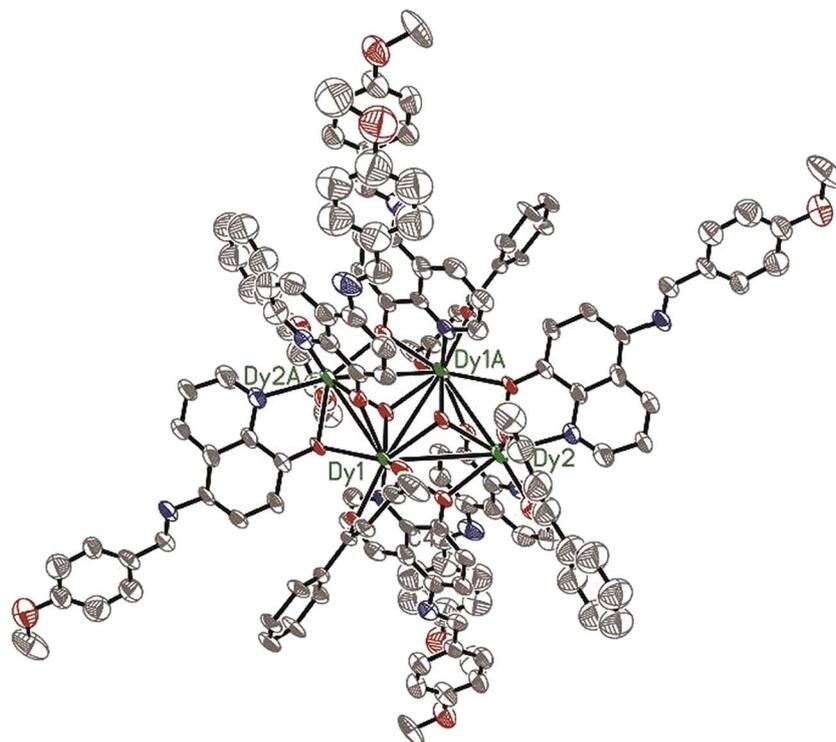

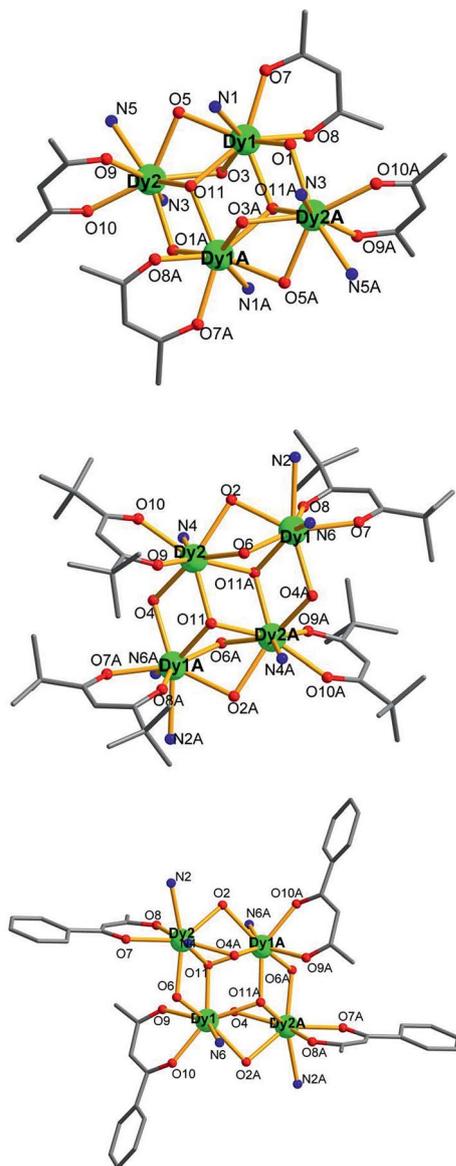**Fig. 4** The molecular structure of compound **10**·Dy. Hydrogen atoms are omitted for clarity (Dy green; C gray; N blue; O red).

Fig. 5 Perspective view of the crystal structures of compounds 3·Dy (top), 9·Dy (middle) and 10·Dy (bottom), with the H atoms and partial HL omitted for clarity.
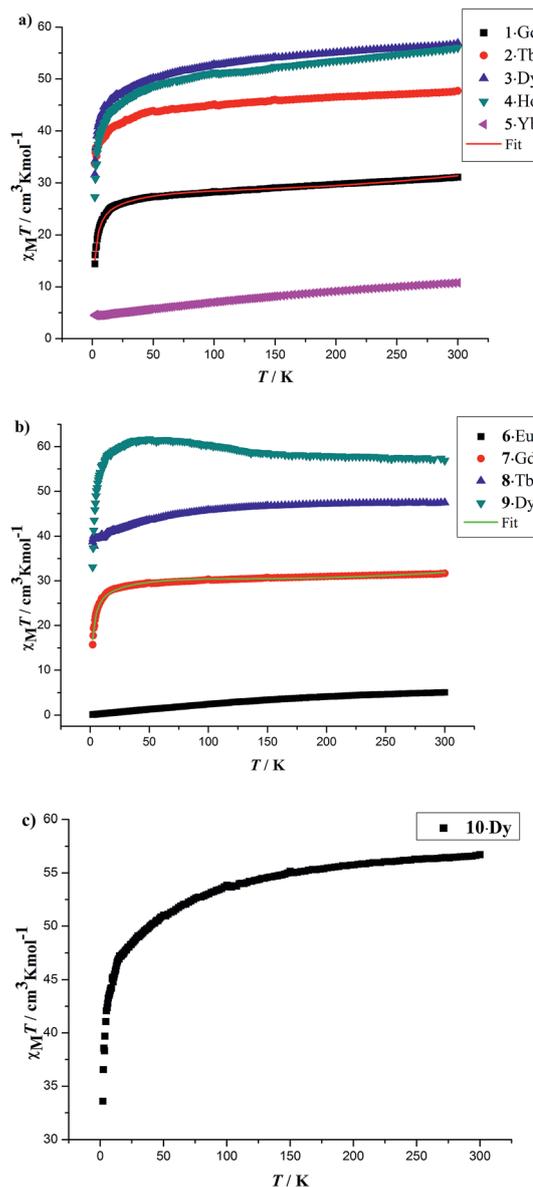

Fig. 6 Temperature dependence of the $\chi_M T$ products at 1000 Oe for 1–5 (a), 6–9 (b) and 10 (c) in the range of 2–300 K. The solid red and green lines are the best fit obtained.

the value of which is much higher than the expected value 0 cm³ K mol⁻¹ for four uncoupled Eu³⁺ (⁷F₀, g = 0), which mainly results from the population of the first and even higher excited states.[16] The $\chi_M T$ value of 6·Eu gradually decrease to 0.10 cm³ K mol⁻¹ at 2 K, basically originating from thermal depopulation of the excited levels. For 7–9, the $\chi_M T$ value at room temperature are 31.67, 47.45 and 56.86 cm³ K mol⁻¹, which are all consistent with the expected values of 31.52, 47.28 and 56.60 cm³ K mol⁻¹ for four isolated Ln³⁺ ions (⁸S₇/₂, g = 2 for Gd³⁺ ions; ⁷F₆, g = 3/2 for Tb³⁺ ions; ⁶H₁₅/₂, g = 4/3 for Dy³⁺ ions). For 7·Gd, different from 1·Gd, the $\chi_M T$ value almost keeps constant up to 20 K, then a sharply decline can be clearly observed, reaching a minimum value of 15.70 cm³ K mol⁻¹ at 2 K. This trend indicates weak antiferromagnetic interaction

exist between adjacent Gd³⁺ ions. For 8·Tb, the $\chi_M T$ value gradually decreases and drop to the minimum value of 38.81 cm³ K mol⁻¹, which can also be ascribed to weak magnetic exchange between Tb³⁺ ions and/or the thermal depopulation of the Tb³⁺ excited Stark sublevels.[17] For 9·Dy, a continuous increase of $\chi_M T$ value upon cooling can be observed up to 50 K, subsequently, a sharp decline to a minimum value of 33.07 cm³ K mol⁻¹ is finally seen at 2 K. This behavior indicates that weak ferromagnetic interactions must dominates between Dy³⁺ ions. For 10·Dy, the plots of $\chi_M T$ vs. T is similar with 1·Gd, the $\chi_M T$ at room temperature 56.72 cm³ K mol⁻¹ are close to the expected value of 56.68 cm³ K mol⁻¹ for four free Dy³⁺ ions. Upon lowering the temperature, the $\chi_M T$ value gradually decreases and then further drops to 33.58 cm³ K mol⁻¹ at 2 K. This trend
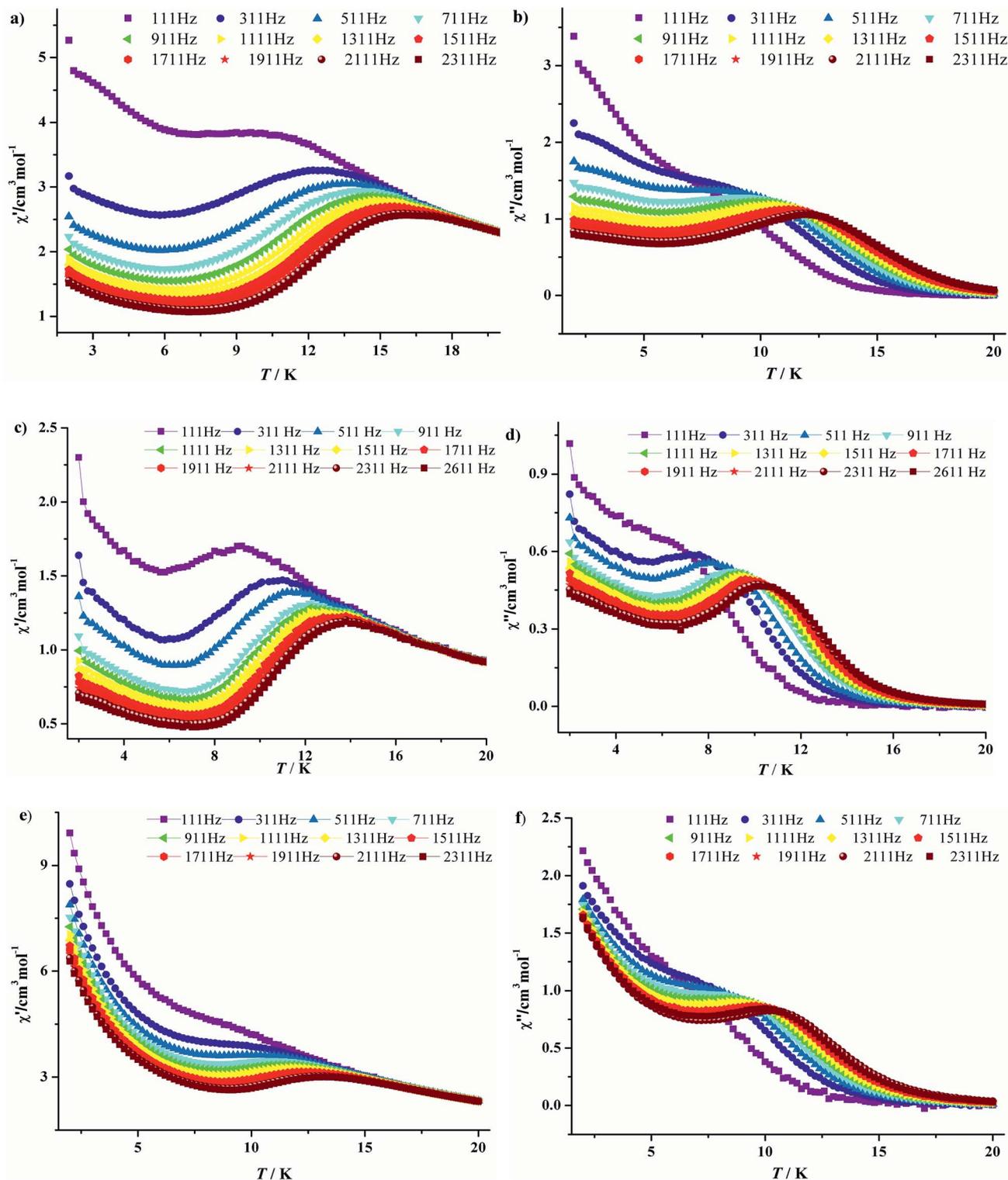
Fig. 7 Temperature-dependent in-phase (χ') and out-phase (χ'') ac susceptibilities plots at different frequencies for **3**·Dy (a, b), **9**·Dy (c, d) and **10**·Dy (e, f).

may be caused by depopulation of the M_J sublevel and anti-ferromagnetic interactions between Dy^{3+} ions. The $\chi_M T$–T plots of **1**·Gd and **7**·Gd were nicely fitted by Hamiltonian (1) with the model in Fig. S5,† giving $g = 1.96$, $J = -0.08$ cm^{-1} and $g = 2.06$,

$J = -0.16$ cm^{-1} for **1**·Gd and **7**·Gd, respectively, the small J values suggest that weak antiferromagnetic interactions exist between adjacent Gd ions. The magnetic susceptibilities of **3**·Dy, **9**·Dy and **10**·Dy fitted by Curie–Weiss law give the Weiss

constants $\theta = -5.41$ for $3 \cdot$Dy, $\theta = 1.93$ for $9 \cdot$Dy and $\theta = -1.27$ for $10 \cdot$Dy (Fig. S6 in ESI†), the positive/negative parameter θ values further confirm the ferromagnetic/antiferromagnetic coupling between Dy^{3+}. Surprisingly, $3 \cdot$Dy, $9 \cdot$Dy and $10 \cdot$Dy, featuring similar Dy_4 clusters, display different magnetic interactions.

$$H_{Gd4} = -J(S_1S_2 + S_3S_4 + S_1S_3 + S_2S_4 + S_1S_4) - g\mu_BH\sum_{i=1}^{4}S_i$$

$$(1)$$

To further investigate the magnetic dynamics of $3 \cdot$Dy, $9 \cdot$Dy and $10 \cdot$Dy, the temperature and frequency dependencies of the alternating current (ac) susceptibilities were performed under 0 direct current and a 3 Oe ac magnetic field (Fig. 7 and 8). Both of the in-phase (χ') and out-of-phase (χ'') signals show strong temperature and frequency dependence as well as remarkable peaks, revealing that all the three tetra-nuclear dysprosium compounds exhibit typical features associated with SMM behaviors. Differently, the χ' and χ'' maximum values of $3 \cdot$Dy are in higher temperature region than that of $9 \cdot$Dy and $10 \cdot$Dy. In addition, the parameter $\varphi = (\Delta T_p/T_p)/\Delta(\log \nu)$ derived from the temperature dependence of in-phase ac susceptibility are 0.21, 0.28 and 0.22 for $3 \cdot$Dy, $9 \cdot$Dy and $10 \cdot$Dy, which are consistent with that of a superparamagnetic, excluding the possibility of spin glass behaviors.[18]
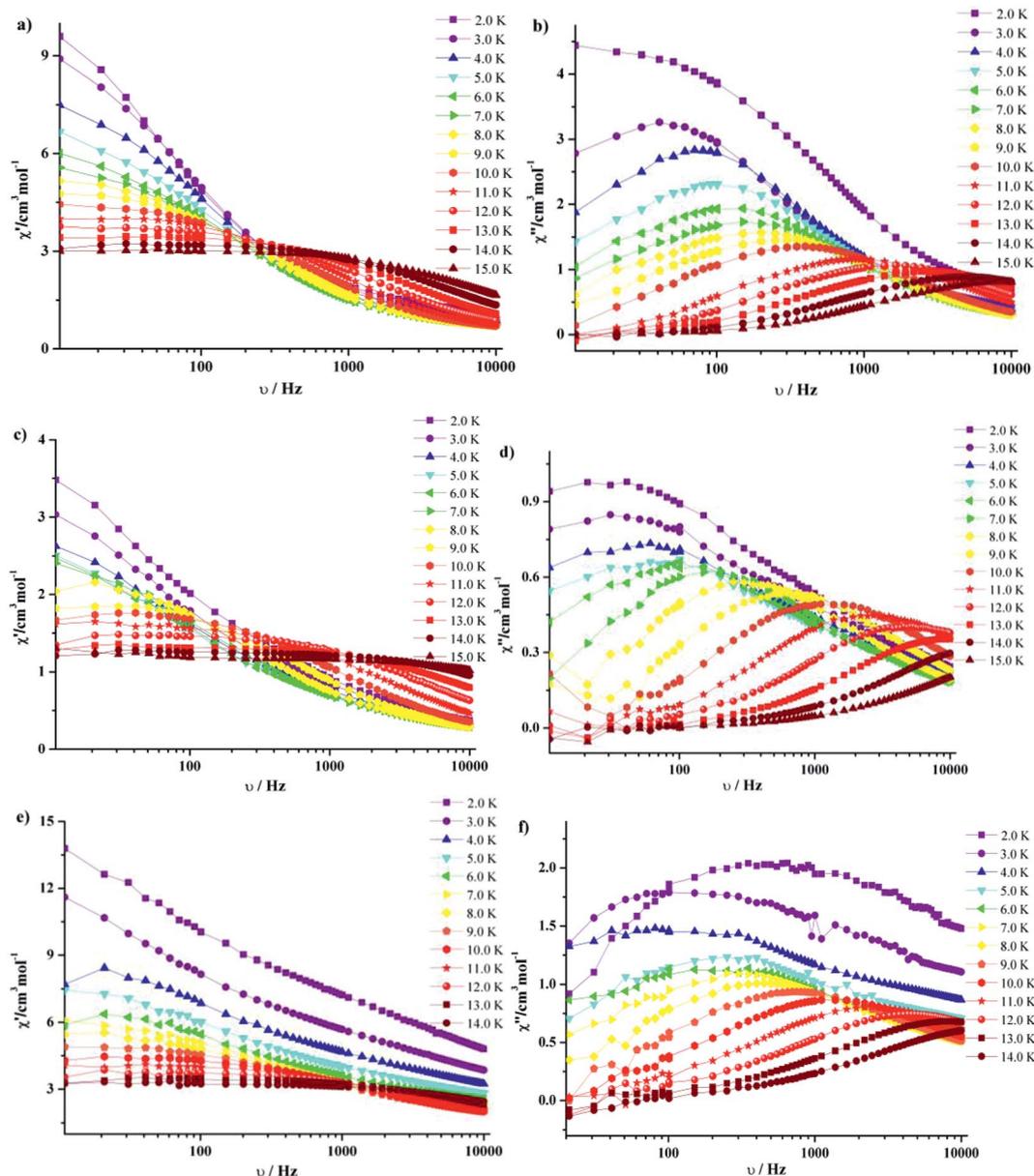

Fig. 8 Frequency dependence of in-phase (χ') and out-phase (χ'') ac susceptibilities at different temperatures for $3 \cdot$Dy (a, b), $9 \cdot$Dy (c, d) and $10 \cdot$Dy (e, f).

It is noteworthy that all the temperature dependencies of ac susceptibilities for $3 \cdot$Dy, $9 \cdot$Dy and $10 \cdot$Dy increase in the lower temperature region, which might be indicative of quantum tunneling effect.[19] To check whether the relaxation processes of them are thermally activated, the relaxation time τ of compounds $3 \cdot$Dy, $9 \cdot$Dy and $10 \cdot$Dy can be derived from the out-of-phase (χ'') peaks in the form of ln τ plotted as a function of $1/T$ (Fig. 9). It is interesting that obvious curvatures in the ln τ vs. $1/T$ plots of $3 \cdot$Dy, $9 \cdot$Dy and $10 \cdot$Dy are observed, indicating a combination of relaxation pathways are operative. As seen from Fig. 8, the relaxation times of them are all temperature

dependent in the whole temperature range, suggesting the relaxation processes are controlled by Orbach and Raman mechanisms rather than the quantum tunneling effects, similar phenomenon is reported by a few SMMs.[20] Given this, the magnetic data of $3 \cdot$Dy, $9 \cdot$Dy and $10 \cdot$Dy can be fitted following the eqn (2) in 2–15 K temperature range.
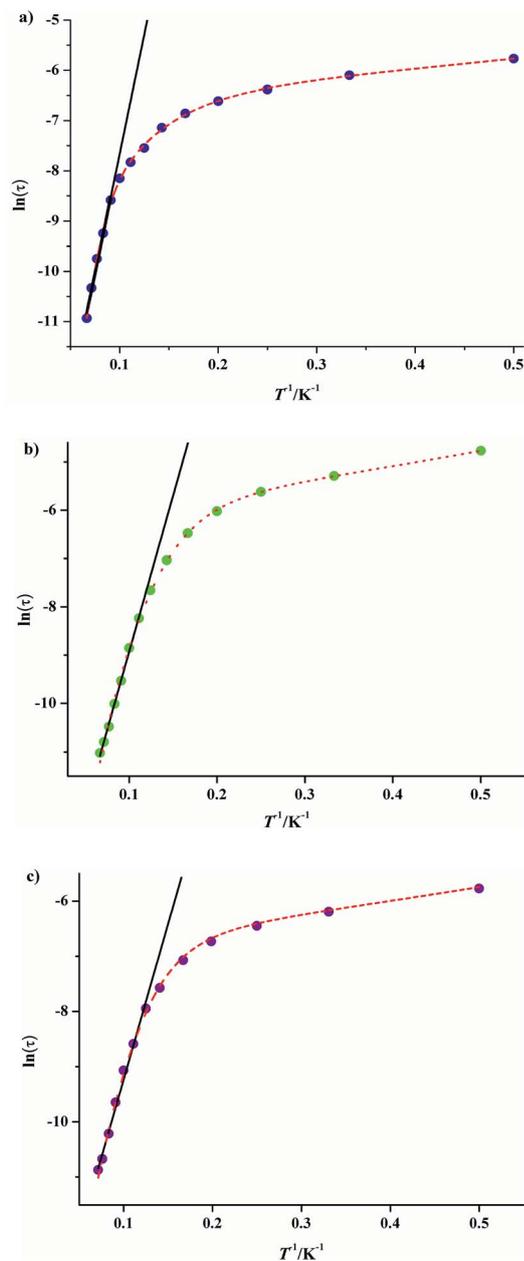
Fig. 9 Temperature dependence of the magnetic relaxation time for $3 \cdot$Dy (a), $9 \cdot$Dy (b) and $10 \cdot$Dy (c), ln(τ) vs. T^{-1} under $H_{dc} = 0$; the solid black lines represent the pure Arrhenius fitting at higher temperature region and the red dashed lines represent the fitting based on eqn (2).

Fig. 10 Cole−Cole plots measured under zero-dc field for $3 \cdot$Dy (a), $9 \cdot$Dy (b) and $10 \cdot$Dy (c). The solid lines are the best fits obtained with a generalized Debye model.

Table 1 The main structural parameters for compounds **3**·Dy, **9**·Dy and **10**·Dy

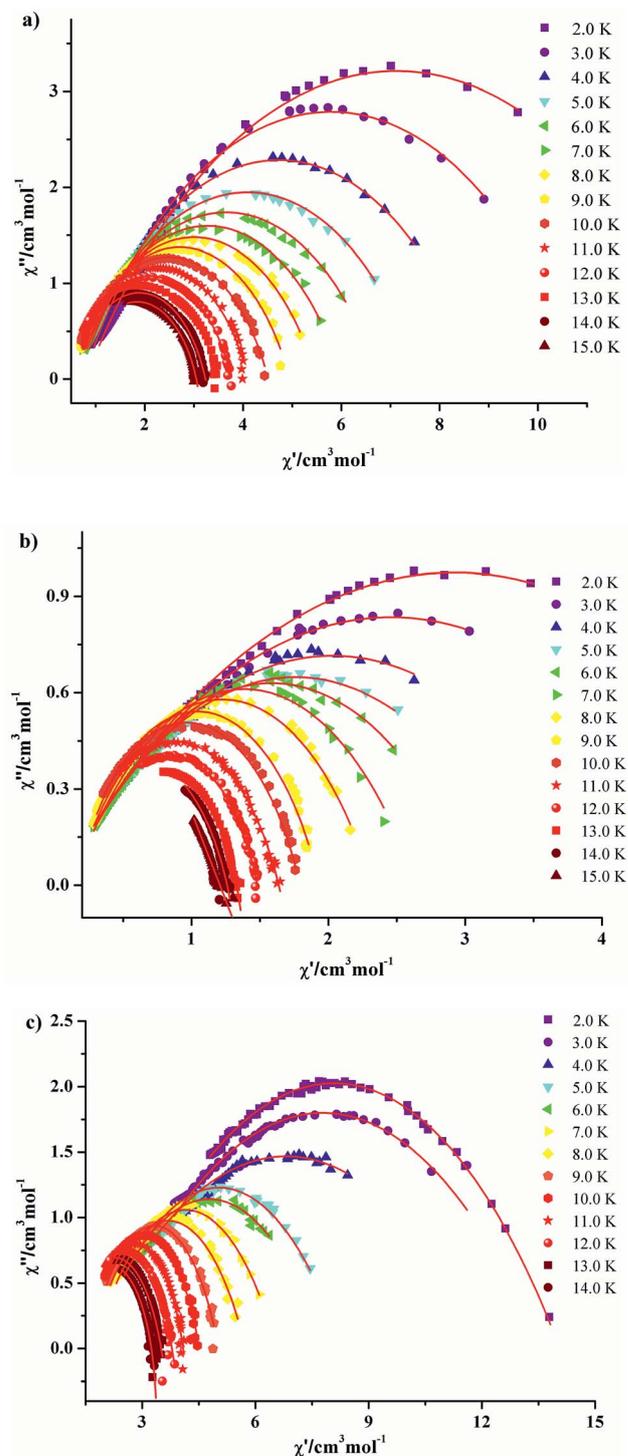| Average distances	Compounds		
	3·Dy	**9**·Dy	**10**·Dy
d(Dy—phenoxide-O) (Å)	2.3801	2.3805	2.4167
d(Dy—μ_3-OH) (Å)	2.3520	2.3649	2.3706
d(Dy—β-diketonate-O) (Å)	2.3068	2.3141	2.3513
d(Dy—N) (Å)	2.5318	2.5466	2.5303
d(Dy–Dy) (Å)	3.7282	3.7473	3.7689

$$\ln \tau = -\ln[AT + B + CT^n + \tau_0^{-1} \exp(-\Delta E/k_B T)] \quad (2)$$

In eqn (2),[21] $AT + B$, CT^n and $\tau_0^{-1} \exp(-\Delta E/k_B T)$ correspond to the direct, Raman and Orbach processes, respectively. The

relaxation energy barriers and pre-exponential factors τ_0 of **3**·Dy, **9**·Dy and **10**·Dy can be obtained by fitting τ values based on the Arrhenius law [$\tau = \tau_0 \exp (\Delta E/k_B T)$] in the high temperature ranges (Fig. 9 black lines), the fitting results give $\Delta E/k_B = 99.29(3)$ K and $\tau_0 = 1.65 \times 10^{-9}$ s for **3**·Dy above 11 K, $\Delta E/k_B = 64.56(4)$ K and $\tau_0 = 2.09 \times 10^{-7}$ s for **9**·Dy above 9 K and $\Delta E/k_B = 61.05(0)$ K and $\tau_0 = 7.99 \times 10^{-7}$ s for **10**·Dy above 8 K. Assuming the value of B is zero, based on the above parameters $\Delta E/k_B$ and τ_0, we successfully fitted the plots $\ln \tau$ vs. $1/T$ in the whole temperature range using eqn (2) with the fitting parameters $n = 3.48, A = 0.4721$ s^{-1} K$^{-3.48}$, $C = 0.8559$ for **3**, $n = 5.64, A = 0.3625$ s^{-1} K$^{-5.64}$, $C = 0.1582$ for **9**·Dy, $n = 5.77, A = 0.4351$ s^{-1} K$^{-5.77}$, $C = 0.139$ for **10**·Dy. The small values of A and C indicate that the relaxation process is dominated by the Orbach and Raman mechanisms at high and low temperature,
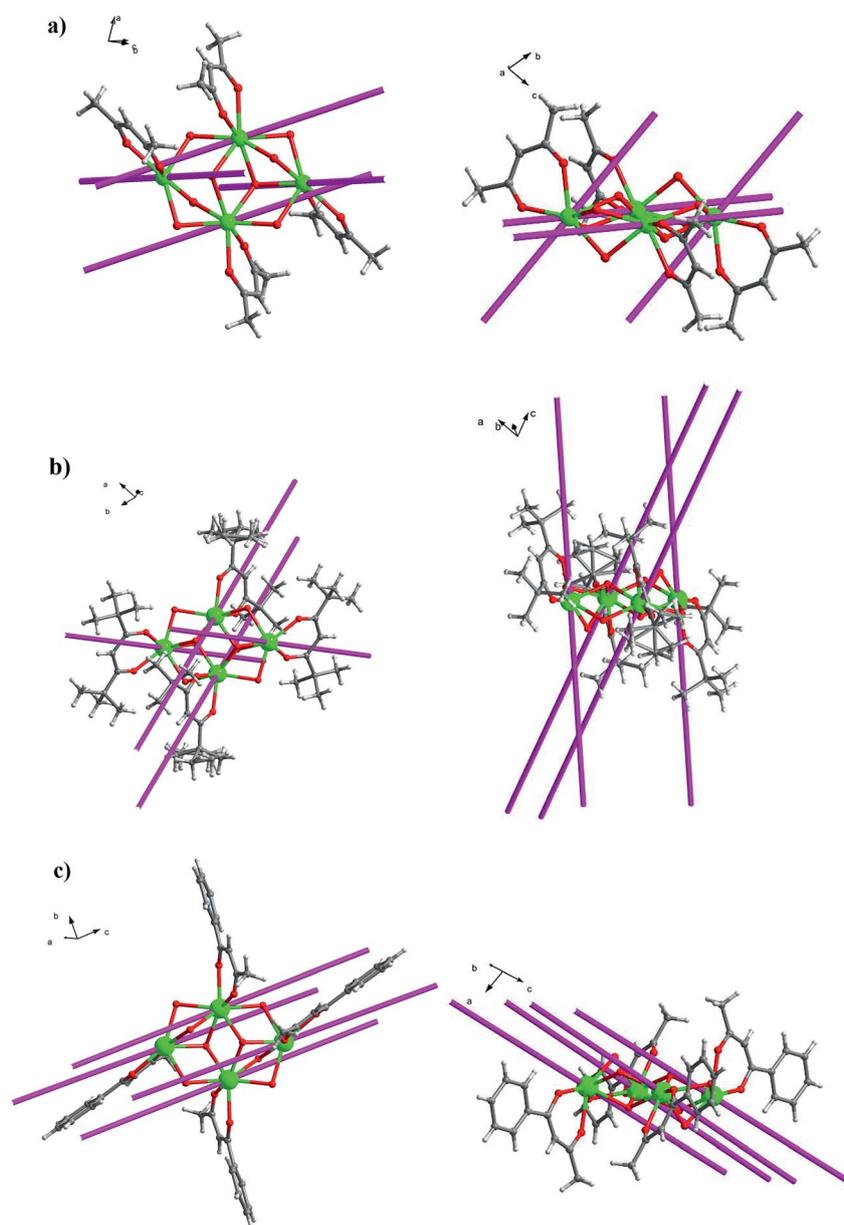

Fig. 11 The magnetic anisotropy easy axes (pink lines) of Dy^{3+} ions in compounds **3**·Dy (a), **9**·Dy (b) and **10**·Dy (c), respectively.

respectively. Interestingly, compounds **3**·Dy, **9**·Dy and **10**·Dy display different relaxation energy barriers, and the value of which are relatively larger in the Dy$_4$ compounds with butterfly shaped arrangements, especially for **3**·Dy. For example, the energy barriers ($\Delta E/k_B$) of them are larger than that of [Dy$_4$(μ$_3$-OH)$_2$(L')$_6$(tmhd)$_4$]·CH$_3$CN (HL' = 5-(4-methylbenzylidene)-8-hydroxylquinoline; Htmhd = 2,2,6,6-tetramethyl-3,5-heptanedione) (46.4 K),[22] [Dy$_4$(μ$_3$-OH)$_2$(L3)$_4$(HL3)$_2$] (H$_2$L3 = (E)-2-(2-hydroxy-3-methoxybenzylideneamino)phenol) (3.7 K),[23] but far lower than the value of [Dy$_4$(μ$_3$-OH)$_2$(bmh)$_2$(msh)$_4$Cl$_2$] (H$_2$bmh = bis(2-hydroxy-3-methoxybenzylidene); Hmsh = 3-methoxysalicylaldehyde hydrazone) (170 K).[5a] The different slow relaxation properties of **3**·Dy, **9**·Dy and **10**·Dy mainly ascribed to the introduction of different β-diketonates, resulting in the slight change of structures in them.

The Cole–Cole diagrams of χ″ *vs.* χ′ with nearly semi-circle shapes for compounds **3**·Dy, **9**·Dy and **10**·Dy are fitted to the generalized Debye model, giving different distribution coefficient α values (Fig. 10). For **3**·Dy, α = 0.25–0.38 was found in the temperature of 2–6 K, while α = 0.27–0.52 (between 2–4 K) and α = 0.30–0.66 (between 2 and 4 K) are obtained for **9**·Dy and **10**·Dy, respectively. The relative larger α value for **10**·Dy indicates that compound **10**·Dy possesses a wider distribution of the relaxation time than **3**·Dy and **9**·Dy. It is noteworthy that three butterfly-shaped tetra-nuclear Dy compounds with similar

arrangements exhibit different magnetic behaviors, which is mainly ascribed to the introduction of different β-diketonates, resulting in the change of crystal fields around center Dy^{3+} ions. In order to investigate the structure–property relationship of **3**·Dy, **9**·Dy and **10**·Dy, some main structural parameters are listed in Table 1, such as the average distance of d(Dy—phenoxide-O) (lengths between Dy^{3+} ions and phenoxide oxygen atoms), d(Dy—μ$_3$-OH) (lengths between Dy^{3+} ions and μ$_3$-OH atoms), d(Dy—β-diketonate-O) (lengths between Dy^{3+} ions and oxygen atoms of β-diketonates), d(Dy–N) (length of Dy–N) and d(Dy—Dy) (length of Dy—Dy). Interestingly, the values of d(Dy—phenoxide-O) and d(Dy—μ$_3$-OH) in the tetranuclear clusters of **3**·Dy, **9**·Dy and **10**·Dy display a continuous increase trend, thus resulting into the shortest distance of Dy—Dy in **3**·Dy and the longest distance of Dy—Dy in **10**·Dy. This tendency is consistent with the fact that stronger interactions occur between adjacent metal ions in **3**·Dy than **9**·Dy and **10**·Dy, as shown in Fig. 6 and S6.† By comparison, the different lengths of d(Dy—β-diketonate-O) observed in **3**·Dy, **9**·Dy and **10**·Dy may be ascribed to the strong steric-hindrance effect of β-diketonates with different substituent groups. The shortest bond lengths of Dy–N/O in **3**·Dy suggests the existence of stronger ligand field around the local Dy^{3+} ions sites. Moreover, as reflected in Fig. 7, the higher block temperature of ac susceptibilities curves observed in **3**·Dy than that in **9**·Dy and **10**·Dy can be also

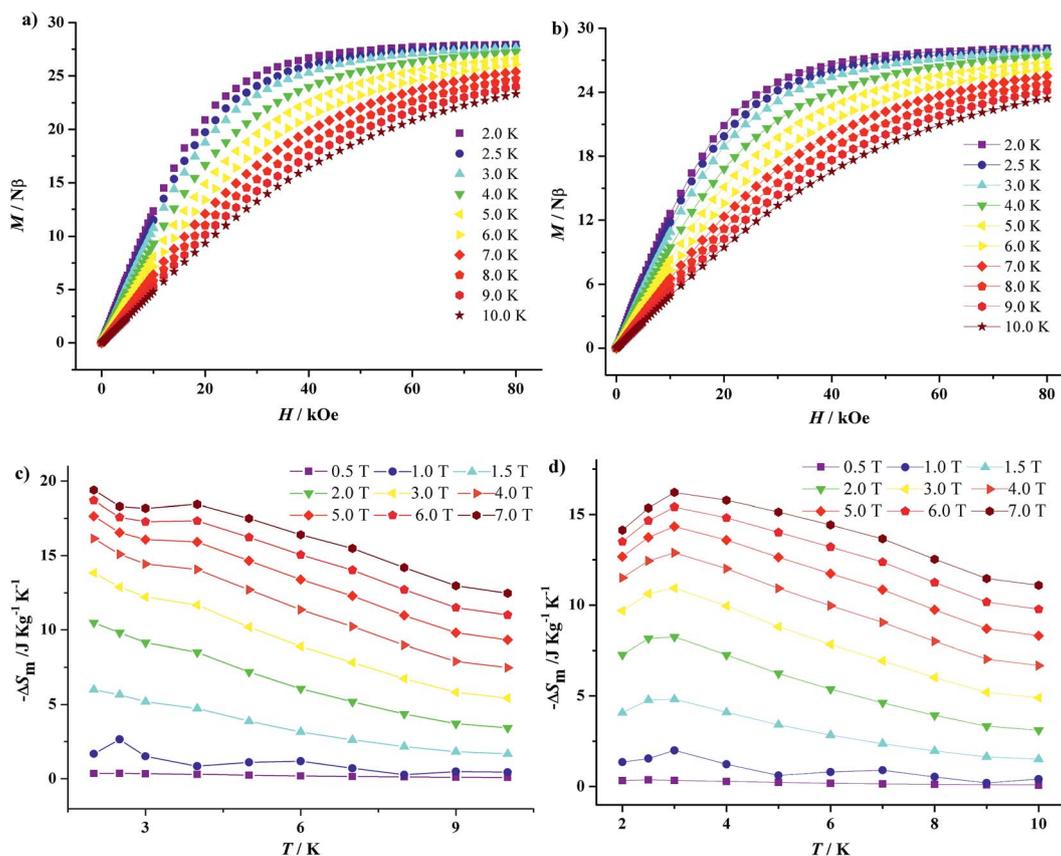**Fig. 12** Magnetization (*M*) *vs.* field (*H*) for **1**·Gd (a) and **7**·Gd (b) in the temperature range of 2–10 K; temperature-dependencies of −Δ*S*$_m$ for **1**·Gd (c) and **7**·Gd (d) obtained from the magnetization data at *T* = 2–10 K and *H* = 0–7 T.

attributed to the stronger ligand field in **3·Dy**. In addition, in order to further investigate the effect of axial ligands on the magnetic properties, the anisotropy axes of the Dy(III) centers in compounds **3·Dy**, **9·Dy** and **10·Dy** have been calculated using the MAGELLAN program (Fig. 11).[24] The results reveal that the orientations of the anisotropy axes for compounds **3·Dy**, **9·Dy** and **10·Dy** are different from each other, their angles between the tetranuclear Dy(III) planes are 39.480° and 88.533° for **3·Dy**, 26.251° and 50.692° for **9·Dy**, 65.515° and 63.916° for **10·Dy**, respectively. It is obvious that the β-diketonates dominate orientation of the anisotropy axes for compounds **3·Dy**, **9·Dy** and **10·Dy**. In view of the above analysis, we conclude that the change of substituent groups of axial ligands play an important role in modulating magnetic behaviors.

Gadolinium with large spin and negligible magnetic anisotropy is a promising candidate to construct magnetic refrigeration materials. Thus, the field-dependent isothermal magnetization curves of **1·Gd** and **7·Gd** are measured in the range of $H = 0$–8 T and $T = 2$–10 K (Fig. 12a and b). The magnetization of **1·Gd** and **7·Gd** display a gradual increase with the increasing field, and reach saturation values of 27.94 Nβ for **1·Gd** and 28.12 Nβ for **7·Gd** at 7 T and 2 K, being close to the theoretical value of 28 Nβ for four Gd^{3+} ($S = 7/2$, $g = 2$) ions.

$$\Delta S_m(T) = \int \left[\partial M(T, H) / \partial T \right]_H dH \tag{3}$$

Additionally, according to the Maxwell eqn (3),[25] the isothermal magnetic entropy change (ΔS_m) of **1·Gd** and **7·Gd** can be obtained (Fig. 12c and d). For **1·Gd**, the maximum value of $-\Delta S_m$ is 19.39(2) J K^{-1} kg^{-1} at 2 K for 7 T without saturation, which is smaller than the expected value of 24.46 J K^{-1} kg^{-1} for four uncoupled Gd^{3+} ions calculated by function of $-\Delta S_m = 4R \ln(2S + 1)$ (R is the gas constant). For **7·Gd**, the value of $-\Delta S_m$ almost keep unchanged with decreasing temperature below 1 T, then it starts to increase rapidly with the external field exceeding 1 T, finally reaching a maximum value of 16.21(3) J K^{-1} kg^{-1} at 3 K for 7 T. The theoretical value is 21.45 J K^{-1} kg^{-1}, the value of which is larger than the experimental one. The gap between the experimental and theoretical values for **1·Gd** and **7·Gd** mainly stemmed from the existence of antiferromagnetic interactions in them.[26] For Gd-based compounds, the magnetocaloric effect is affected by M_w/N_{Gd} and θ. As shown in Table 2, compound **1·Gd** and **7·Gd** have different values of M_w/N_{Gd} and θ, the values of M_w/N_{Gd} and $|\theta|$ for **1·Gd** are smaller than **7·Gd**, indicating that **1·Gd** have a larger magnetic density and weaker magnetic coupling. Thus, the $-\Delta S_m$ value of **1·Gd** is larger than that of **7·Gd**. However, the $-\Delta S_m$ values of them are both smaller than tetra-nuclear Gd^{3+} compound [Gd$_4$-

$(OAc)_4(acac)_8(H_2O)_4$] (37.7 J K^{-1} kg^{-1} at 2 K for 7 T) with smaller value of M_w/N_{Gd} radio (432.53) and weak ferromagnetic interactions θ (0.23).[27] Hence, the selection of low molecular weight ligands that lead to weak interaction is a promising way for constructing Gd^{3+} based magnetic refrigeration materials.

Conclusion

In summary, ten new tetranuclear lanthanide compounds have been successfully designed by using Schiff base ligand HL and three different β-diketonate auxiliary ligands. Compounds **1–10** all consist of butterfly-shaped planar tetranuclear clusters, and the Ln$_4$O$_2$ cores are encapsulated inside the same coordination pockets [O$_{14}$N$_6$]. Magnetic investigations reveal that compounds **1·Gd** and **7·Gd** display different magnetocaloric effects ($-\Delta S_m^{max} = 19.39(2)$ J K^{-1} kg^{-1} for **1·Gd** and 16.21(3) J K^{-1} kg^{-1} for **7·Gd**) due to their divergence in M_w/N_{Gd} ratios and magnetic interaction. In addition, compounds **3·Dy**, **9·Dy** and **10·Dy** display different magnetic dynamic behaviors in spite of their similar structures. A simple comparative investigation uncovers that the introduction of different substituent groups in β-diketonate auxiliary ligands result in the change of magnetic anisotropy of Dy^{3+} centers in them, and thus give rise to the difference of magnetic relaxation behaviors in this system. Given the versatility of the β-diketonates, we plan to regulate their structures and magnetic properties in other types of polynuclear Ln-clusters to further investigate the inner structure–properties relationship more deeply. This work provides an important path in the fine-tuning of the magnetic properties of SMMs. We believe that this work not only present to us various polynuclear Ln^{3+} clusters but also provide an inspiration in modulating magnetic dynamic behaviors of Ln-based SMMs, further stimulating investigation on the slow relaxation mechanism.

Conflicts of interest

There are no conflicts to declare.

Acknowledgements

Notes and references

1 (*a*) C. Dossantos, A. Harte, S. Quinn and T. Gunnlaugsson, *Coord. Chem. Rev.*, 2008, **252**, 2512–2527; (*b*) S. Sanvito, *Chem. Soc. Rev.*, 2011, **40**, 3336–3355.

2 (*a*) J. C. G. Bünzli, *Chem. Rev.*, 2010, **110**, 2729–2755; (*b*) S. Hill, R. S. Edwards, N. Aliaga-Alcalde and G. Christou, *Science*, 2003, **302**, 1015–1018.

3 (*a*) E. Saitoh, H. Miyajima, T. Yamaoka and G. Tatara, *Nature*, 2004, **432**, 203–206; (*b*) M. Y. Wu, F. L. Jiang, X. J. Kong,

Table 2 Comparison of the $-\Delta S_m^{max}$ values of **1·Gd** and **7·Gd**

Compounds	M_w/N_{Gd}	Magnetic interaction [θ, K]	$-\Delta S_m^{max}$ [J kg^{-1}K^{-1}]
1·Gd	680.8	−2.92	19.39(2)
7·Gd	808.5	−3.35	16.21(3)

D. Q. Yuan, L. S. Long, S. A. Al-Thabaiti and M. C. Hong, *Chem. Sci.*, 2013, **4**, 3104–3109.

4 (*a*) S. Y. Lin, X. L. Li, H. S. Ke and Z. K. Xu, *CrystEngComm*, 2015, **17**, 9167–9174; (*b*) H. L. Gao, L. Jiang, H. Y. Shen, W. M. Wang and J. Z. Cui, *Dalton Trans.*, 2016, **45**, 253–264; (*c*) C. A. P. Goodwin, F. Ortu, D. Reta, N. F. Chilton and D. P. Mills, *Nature*, 2017, **548**, 439–442.

5 (*a*) P. H. Lin, T. J. Burchell, L. Ungur, L. F. Chibotaru, W. Wernsdorfer and M. Murugesu, *Angew. Chem., Int. Ed.*, 2009, **48**, 9489–9492; (*b*) Q. Y. Liu, Y. L. Li, W. L. Xiong, Y. L. Wang, F. Luo, C. M. Liu and L. L. Chen, *CrystEngComm*, 2014, **16**, 585–590; (*c*) F. S. Guo, B. M. Day, Y. C. Chen, M. L. Tong, A. Mansikkamäki and R. A. Layfield, *Angew. Chem., Int. Ed.*, 2017, **56**, 11445–11449.

6 (*a*) Y. X. Wang, W. Shi, H. Li, Y. Song, L. Fang, Y. H. Lan, A. K. Powell, W. Wernsdorfer, L. Ungur, L. F. Chibotaru, M. R. Shen and P. Cheng, *Chem. Sci.*, 2012, **3**, 3366–3370; (*b*) J. Liu, Y. C. Chen, Z. X. Jiang, J. L. Liu, J. H. Jia, L. F. Wang, Q. W. Li and M. L. Tong, *Dalton Trans.*, 2015, **44**, 8150–8155; (*c*) S. K. Langley, N. F. Chilton, I. A. Gass, B. Moubaraki and K. S. Murray, *Dalton Trans.*, 2011, **40**, 12656–12659; (*d*) E. M. Pineda, Y. H. Lan, O. Fuhr, W. Wernsdorfer and M. Ruben, *Chem. Sci.*, 2017, **8**, 1178–1185.

7 (*a*) S. D. Jiang, B. W. Wang, G. Su, Z. M. Wang and S. Gao, *Angew. Chem., Int. Ed.*, 2010, **49**, 7448–7451; (*b*) L. Zhao, J. F. Wu, H. S. Ke and J. K. Tang, *CrystEngComm*, 2013, **15**, 5301–5306; (*c*) Y. L. Wang, N. Zhou, Y. Ma, Z. X. Qin, Q. L. Wang, L. C. Li, P. Cheng and D. Z. Liao, *CrystEngComm*, 2012, **14**, 235–239.

8 (*a*) J. Y. Ge, H. Y. Wang, J. Li, J. Z. Xie, Y. Song and J. L. Zuo, *Dalton Trans.*, 2017, **46**, 3353–3362; (*b*) W. Huang, F. X. Shen, S. Q. Wu, L. Liu, D. Wu, Z. Zheng, J. Xu, M. Zhang, X. C. Huang, J. Jiang, F. Pan, Y. Li, K. Zhu and O. Sato, *Inorg. Chem.*, 2016, **55**, 5476–5484.

9 (*a*) Y. W. Li, S. J. Liu, T. L. Hu and X. H. Bu, *Dalton Trans.*, 2014, **43**, 11470–11473; (*b*) A. Nandy and S. K. Pradhan, *Dalton Trans.*, 2015, **44**, 17229–17240.

10 L. F. Zou, L. Zhao, P. Chen, Y. N. Guo, Y. Guo, Y. H. Li and J. K. Tang, *Dalton Trans.*, 2012, **41**, 2966–2971.

11 J. Liu, Y. C. Chen, J. L. Liu, V. Vieru, L. Ungur, J. H. Jia, L. F. Chibotaru, Y. H. Lan, W. Wernsdorfer, S. Gao, X. M. Chen and M. L. Tong, *J. Am. Chem. Soc.*, 2016, **138**, 5441–5450.

12 P. Zhang, L. Zhang, S. Y. Lin, S. F. Xue and J. K. Tang, *Inorg. Chem.*, 2013, **52**, 4587–4592.

13 W. M. Wang, W. Z. Qiao, H. X. Zhang, S. Y. Wang, Y. Y. Nie, H. M. Chen, Z. Liu, H. L. Gao, J. Z. Cui and B. Zhao, *Dalton Trans.*, 2016, **450**, 8182–8191.

14 (*a*) H. L. Gao, L. Jiang, W. M. Wang, S. Y. Wang, H. X. Zhang and J. Z. Cui, *Inorg. Chem.*, 2016, **55**, 8898–8904; (*b*) S. Katagiri, Y. Tsukahara, Y. Hasegawa and Y. Wada, *Bull. Chem. Soc. Jpn.*, 2007, **80**, 1492–1503.

15 I. Nemec, M. Machata, R. Herchel, R. Boča and Z. Trávníček, *Dalton Trans.*, 2012, **41**, 14603–14610.

16 Y. L. Hou, G. Xiong, B. Shen, B. Zhao, Z. Chen and J. Z. Cui, *Dalton Trans.*, 2013, **42**, 3587–3596.

17 (*a*) L. Zhang, P. Zhang, L. Zhao, J. F. Wu, M. Guo and J. K. Tang, *Dalton Trans.*, 2016, **45**, 10556–10562; (*b*) X. L. Li, H. Li, D. M. Chen, C. Wang, J. F. Wu, J. K. Tang, W. Shi and P. Cheng, *Dalton Trans.*, 2015, **44**, 20316–20320.

18 D. P. Dong, Y. J. Zhang, H. Zheng, P. F. Zhuang, L. Zhao, Y. Xu, J. X. Hu, T. Liu and C. Y. Duan, *Dalton Trans.*, 2013, **42**, 7693–7698.

19 (*a*) P. H. Lin, W. B. Sun, M. F. Yu, G. M. Li, P. F. Yan and M. Murugesu, *Chem. Commun.*, 2011, **47**, 10993–10995; (*b*) N. Ishikawa, M. Sugita, N. Tanaka, T. Ishikawa, S. Y. Koshihara and Y. Kaizu, *Inorg. Chem.*, 2004, **43**, 5498–5500.

20 (*a*) D. Zhang, Y. M. Tian, W. B. Sun, H. F. Li, P. Chen, Y. Q. Zhang and P. F. Yan, *Dalton Trans.*, 2016, **45**, 2674–2680; (*b*) S. Titos-Padilla, J. Ruiz, J. M. Herrera, E. K. Brechin, W. Wernsdorfer, F. Lloret and E. Colacio, *Inorg. Chem.*, 2013, **52**, 9620–9626; (*c*) W. B. Sun, B. Yan, Y. Q. Zhang, B. W. Wang, Z. M. Wang, J. H. Jia and S. Gao, *Inorg. Chem. Front.*, 2014, **1**, 503–509.

21 K. R. Meihaus, S. G. Minasian, W. W. Lukens, S. A. Kozimor, D. K. Shuh, T. Tyliszczak and J. R. Long, *J. Am. Chem. Soc.*, 2014, **136**, 6056–6068.

22 Z. L. Wu, Y. G. Ran, X. Y. Wu, Y. P. Xia, M. Fang and W. M. Wang, *Polyhedron*, 2017, **126**, 282–286.

23 K. C. Mondal, G. E. Kostakis, Y. H. Lan and A. K. Powell, *Polyhedron*, 2013, **66**, 268–273.

24 N. F. Chilton, D. Collison, E. J. L. McInnes, R. E. P. Winpenny and A. Soncini, *Nat. Commun.*, 2013, **4**, 2551.

25 (*a*) G. Karotsis, M. Evangelisti, S. J. Dalgarno and E. K. Brechin, *Angew. Chem., Int. Ed.*, 2009, **48**, 9928–9931; (*b*) M. Evangelisti, F. Luis, L. De Jongh and M. Affronte, *J. Mater. Chem.*, 2006, **16**, 2534–2549.

26 (*a*) J. B. Peng, Q. C. Zhang, X. J. Kong, Y. P. Ren, L. S. Long, R. B. Huang, L. S. Zheng and Z. Zheng, *Angew. Chem., Int. Ed.*, 2011, **50**, 10649–10652; (*b*) J. M. Jia, S. J. Liu, Y. Cui, S. D. Han, T. L. Hu and X. H. Bu, *Cryst. Growth Des.*, 2013, **13**, 4631–4634.

27 F. S. Guo, J. D. Leng, J. L. Liu, Z. S. Meng and M. L. Tong, *Inorg. Chem.*, 2012, **51**, 405–413.